Soft Matter

Confined active matter in external fields

Journal:	*Soft Matter*
Manuscript ID	SM-ART-08-2022-001135.R1
Article Type:	Paper
Date Submitted by the Author:	24-Dec-2022
Complete List of Authors:	Shaik, Vaseem; The University of British Columbia, Mechanical Engineering Peng, Zhiwei; California Institute of Technology, Division of Chemistry and Chemical Engineering Brady, John; California Institute of Technology, Division of Chemistry and Chemical Engineering Elfring, Gwynn; University of British Columbia,

Soft Matter

ARTICLE TYPE

Cite this: DOI: 00.0000/xxxxxxxxxx

Confined active matter in external fields†

Vaseem A. Shaik,[a] Zhiwei Peng,[b] John F. Brady,[b] and Gwynn J. Elfring*[a]

Received Date
Accepted Date

DOI: 00.0000/xxxxxxxxxx

We analyze a dilute suspension of active particles confined between walls and subjected to fields that can modulate particle speed as well as orientation. Generally, the particle distribution is different in the bulk compared to near the walls. In the bulk, particles tend to accumulate in the regions of low speed, but in the presence of an orienting field normal to the walls, particles rotate to align with the field and accumulate in the field direction. At the walls, particles tend to accumulate pointing into the walls and thereby exert pressure on walls. But the presence of strong orienting fields can cause the particles to reorient away from the walls, and hence shows a possible mechanism for preventing contamination of surfaces. The pressure at the walls depends on the wall separation and the field strengths. This work demonstrates how multiple fields with different functionalities can be used to control active matter under confinement.

1 Introduction

Active matter refers to a suspension of active particles that convert stored energy to directed motion[1–5]. Examples include a school of fish, a flock of birds and a suspension of microorganisms. Our focus here is on active matter systems where the active particles are micron sized and hence the inertia of the particles and the induced flow is negligible. Such active matter systems exhibit rich phenomena due to the self-propelling constituents, including collective motion[6], active turbulence[7] and motility-induced phase separation[8].

The dynamics of active particles depend on characteristics such as their speed[9–13], orientation[14] and diffusivity[15], and thus a degree of control over active matter can be exerted through modulation of these properties. By subjecting active particles to external fields like magnetic fields or gravitational fields or even gradients in heat, light or fluid viscosity, active particles have been shown to perform *taxis* either by rotating to align with the external field or speeding up (or slowing down) in the field, or both. An example is *Chlamydomonas nivalis* which reorients to preferentially swim against gravity due to bottomheaviness[16]. More impressively, one can 'paint' with the bacterium *E. coli* by exposing the bacterial suspension to the light gradients[17] as the bacterium changes its speed in response to light. More sophisticated control of synthetic active matter has recently been demonstrated by employing external magnetic fields and discrete-time feedback loops to tune the rotational diffusivity of active colloids[15]. It is in this vein, namely controlling the dynamics of active matter, that we develop theory for confined active particles subject to fields that can modulate particle speed as well as orientation.

Several researchers have analyzed the dynamics of active particles with spatially varying speeds[8,18–22]. When the spatial variation is slow and restricted to 1D, the number density n and the swim speed U are shown to be inversely proportional, $nU = constant$[18]. This relation means that particles accumulate in the regions of low speed and has been shown to apply to active matter under abrupt speed changes provided that (thermal or biological) fluctuations are relatively weak[22].

Active particles also tend to accumulate at confining boundaries due to their directional persistence[23,24], they tend to point into the walls and exert a force (or pressure) on these confining boundaries. This pressure usually depends on the precise microscopic and hydrodynamic interactions between the particles and the boundary[25,26]. In the absence of any external field, it is a sum of the bulk osmotic pressure and the swim pressure[27], which is the unique pressure required to confine particles[28]. If an orienting field is also present then the particles rotate to align with the field, nonzero net polar order develops in the entire domain and boundary accumulation is modified[24]. Net polar order gives rise to a net average swim force and the wall pressure in this case is a sum of the swim pressure and the effective body force due to reorientation that acts on particles[24]. It has also been shown that in a bipolar orienting field, particles rotate to align along as well as against the field. This results in zero polar order but net nematic order. In such fields, the swim stress was shown to be tensorial and hence, the wall pressure is the wall normal component of the swim stress[29]. Computational simulations of active particles

[a] *Department of Mechanical Engineering, Institute of Applied Mathematics, University of British Columbia, Vancouver, BC, V6T 1Z4, Canada.*
Email: gelfring@mech.ubc.ca
[b] *Division of Chemistry and Chemical Engineering, California Institute of Technology, Pasadena, California 91125, USA.*

† Electronic Supplementary Information (ESI) available: See DOI: 10.1039/xxxxxxxxxx/

in the presence of orienting fields have also revealed how such fields can drive steady unidirectional internal flows[30].

Spatial variation of the speed of active particles as well as an induced reorientation can also be caused by subjecting the particles to external flows. Indeed, the dynamics of confined active particles in the presence of external flows is relatively well explored. Diverse phenomena such as upstream swimming[31–35], shear trapping and center line depletion[23,36], and a non-monotonic variation of longitudinal dispersivity with the flow rate[35,37] have all been observed and described. Theoretical approaches for deriving macroscale transport properties include generalized Taylor dispersion theory[38] and recently a local approximation model for macroscale transport[39]. The complications associated with an additional orienting field, such as gravity acting on bottom-heavy particles[16,40], or the chemical gradients acting on chemotactic particles[41], have also been analyzed. If the external field is prescribed and particles do not disturb the background flow, these systems have a similar mathematical structure to the system we consider here. But there are several differences. First, the motivation in our case is in exerting simple control of active particles to achieve rectified dynamics through the use of external fields. Particle dynamics in external flows is usually quite different, for instance a particle in shear or Poiseuille flow will rotate continuously exhibiting periodic dynamics between walls[35,42]. Also, we conduct a full boundary-layer analysis of the number density and polar order fields of active particles (under forcing) near walls at the high Péclet numbers that are often most relevant.

While particle speed and orientation can both be controlled by external fields[28], theory has not yet been developed for confined active matter subjected to external fields that modulate both. Specifically, the scaling law satisfied by the number density is not known, and thus previous experimental work compared results with the $nU = constant$ scaling law[43]. Also, the only theory developed in previous work for the confined active matter in the presence of a orienting field was valid for wall separations much larger than the run length, which is the distance an active particle travels before reorienting due to the rotary Brownian motion[24]. Here we derive theory for active matter subjected to the two aforementioned fields, valid in the relevant limit of weak translational Brownian motion (or high activity[44]) and for all wall separations relative to the run length. We solve for the number density and wall pressure, as well as probe the theory and underlying physics that impact wall accumulation.

2 Confined active particles

2.1 Active Brownian particles

We consider a dilute suspension of active particles confined between two infinite plane walls that are separated by a distance L. See Fig. 1 for the schematic. The particles are subjected to an external field that modulates the particles' speed spatially $\mathbf{U} = U(\mathbf{x})\mathbf{q}$, where the unit vector $\mathbf{q}$ is the particle orientation. This can be achieved by imposing light on photo-sensitive bacteria or synthetic robots or even by spatially varying the 'fuel' that bacteria consume. The particles are also subject to an external field that leads to reorientation to align with the field direction

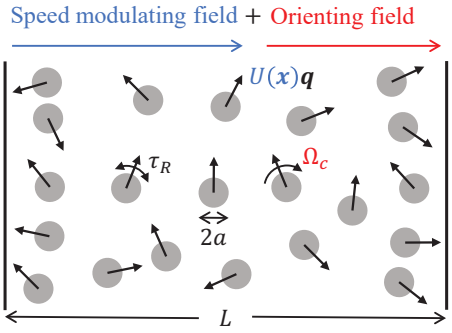

Fig. 1 A dilute suspension of spherical active particles of radius a confined between two walls that are separated by a distance L. The particles are subjected to a field that modulates their speed spatially $\mathbf{U} = U(\mathbf{x})\mathbf{q}$ and also to a field that rotates them at a rate $|\Omega_c|$. Additionally, particles undergo rotational diffusion with a time scale $\tau_R = 1/D_R$.

$\hat{\mathbf{H}}$. This reorientation can be caused by imposing magnetic or gravitational fields on the magnetotactic or bottom heavy bacteria, respectively, or even by spatially varying the background fluid viscosity[45,46]. The rate of reorientation is quantified by a characteristic angular velocity $\mathbf{\Omega} = \Omega_c(\mathbf{q} \times \hat{\mathbf{H}})$, that is determined from the balance between torque caused by the field (which may be hydrodynamic or external depending on the particular mechanism driving reorientation) and rotational drag. For simplicity and with no lack of generality we assume the characteristic rate $\Omega_c > 0$.

The particles are subject to fluctuations that lead to translational and rotational diffusion with diffusivities, D_T and D_R, respectively. The fluctuations may be thermal or biological in origin but regardless of the origin we consider the diffusivities to be constant and independent of the imposed background fields. Importantly, the particles in our model do not interact with one another, hydrodynamically or otherwise. This simple model of active particles is called the active Brownian particle (ABP) model and it has been used widely to understand various phenomena without any hydrodynamic interactions[3].

2.2 Smoluchowski analysis

The probability of finding a particle in the vicinity of position $\mathbf{x}$, and orientation $\mathbf{q}$ at time t, $P(\mathbf{x},\mathbf{q},t)\,d\mathbf{x}d\mathbf{q}$, is governed by the Smoluchowski equation

$$\frac{\partial P}{\partial t} + \nabla \cdot \mathbf{j}_T + \nabla_R \cdot \mathbf{j}_R = 0, \tag{1}$$

where $\nabla_R = \mathbf{q} \times \partial/\partial\mathbf{q}$ and the translational and rotational fluxes are $\mathbf{j}_T = \mathbf{U}P - D_T\nabla P$ and $\mathbf{j}_R = \mathbf{\Omega}P - D_R\nabla_R P$, respectively[47]. The particles are prevented from entering the walls by enforcing zero translational flux normal to the walls $\mathbf{n} \cdot \mathbf{j}_T|_{\text{wall}} = 0$, where $\mathbf{n}$ is the unit vector normal to the wall. The total number of particles is conserved by requiring that $\int\int P d\mathbf{q}d\mathbf{x} = 1$.

To capture the essential physics, we focus on the orientational moments of the probability density $P(\mathbf{x},\mathbf{q},t)$. The first few moments are the number density $n = \int P d\mathbf{q}$, the polar order $\mathbf{m} = \int P\mathbf{q}d\mathbf{q}$, and the nematic order $\mathbf{Q} = \int P\left(\mathbf{qq} - \frac{\mathbf{I}}{d}\right)d\mathbf{q}$, where d is the dimensionality of the problem. These moments emerge naturally

expanding the probability density in terms of the irreducible tensors of the orientation $\mathbf{q}$, $P(\mathbf{x},\mathbf{q},t) = n + \mathbf{m}\cdot\mathbf{q} + \mathbf{Q} : \overline{\mathbf{qq}} + O\left(\overline{\mathbf{qqq}}\right)$. The overbracket denotes the irreducible part of a tensor[48], for example $\overline{\mathbf{qq}} = \mathbf{qq} - \mathbf{I}/d$. Equations governing these moments can be derived by projecting (1) onto the basis of these irreducible tensors. Hence, n and $\mathbf{m}$ satisfy

$$\frac{\partial n}{\partial t} + \nabla\cdot\mathbf{j}_n = 0, \tag{2}$$

$$\frac{\partial \mathbf{m}}{\partial t} + \nabla\cdot\mathbf{j}_m + \Omega_c\hat{\mathbf{H}}\cdot\mathbf{Q} - \Omega_c n\hat{\mathbf{H}}\left(1-\frac{1}{d}\right) + D_R(d-1)\mathbf{m} = \mathbf{0}, \tag{3}$$

where,

$$\mathbf{j}_n = \int \mathbf{j}_T\, d\mathbf{q} = U(\mathbf{x})\,\mathbf{m} - D_T\nabla n, \tag{4}$$

$$\mathbf{j}_m = \int \mathbf{j}_T\,\mathbf{q} d\mathbf{q} = U(\mathbf{x})\,\mathbf{Q} + \frac{nU(\mathbf{x})}{d}\mathbf{I} - D_T\nabla\mathbf{m}. \tag{5}$$

Additionally, moments of the no-flux condition at the walls $\mathbf{n}\cdot\mathbf{j}_T|_{\text{wall}} = 0$ yield $\mathbf{n}\cdot\mathbf{j}_n|_{\text{wall}} = 0$ and $\mathbf{n}\cdot\mathbf{j}_m|_{\text{wall}} = 0$, for the first two moments. Finally, the integral constraint $\int\int P d\mathbf{q} d\mathbf{x} = 1$ implies $\int n\, d\mathbf{x} = 1$. A closure problem immediately arises due to fluxes of a particular moment depending the next (higher) moment. The approximation used here to close these equations and its validity are discussed in the next section.

We note that the choice of boundary condition that enforces particle number conservation is not unique. A weaker boundary condition imposing no-flux only on the number density can be used[41] and the choice of boundary conditions affects the number density distribution and other derived macrotransport properties[49]. Our point of view is that the boundary conditions of the Smoluchowski equation should be based on the micromechanics of the particle-wall interaction, in order to accurately capture the intended physical picture. In particular, in the absence of hydrodynamic interactions as we consider here, this particle-wall interaction is the steric interaction between a hard particle and a hard wall and the no-flux condition originates from the contact dynamics between a particle and the wall. When the sphere is in contact with a planar wall, the wall exerts a force that is normal to the spherical surface at the single point of contact. When the sphere is not in contact with the wall, the force vanishes. For an active sphere, regardless of the orientation that it comes into contact with the wall, the direction of the force always points toward the center of the sphere. This ultimately leads to a no-flux condition must be satisfied for all orientations. One can derive this by considering a repulsive potential and then performing a matched-asymptotic analysis in the limit that the potential approaches that of a hard wall (Peng & Brady, unpublished).

2.3 Analysis

We begin first by examining the relevant physical scales in the problem. There are two time scales: the reorientation time, $\tau_R = 1/D_R$, due to rotary Brownian motion or some internal biological mechanism, and the time that the field takes to reorient the particle $1/\Omega_c$. There are also three length scales: the microscopic length $\delta = \sqrt{D_T\tau_R}$, the run length $\ell = U_0\tau_R$, and the channel width L, where U_0 is the self-propulsion speed in the absence of fields. The governing equations are ultimately characterized by four dimensionless numbers: the channel gap relative to run length L/ℓ, the Péclet number $\text{Pe} = U_0\ell/D_T$ measuring the ratio of the self-advective (i.e., swimming) to the diffusive transport rate of particles, and two dimensionless groups which give the relative magnitude of the effects of the external fields: the relative importance of variations in speed $\alpha_L = \Delta U/U_0$, where ΔU is the characteristic change in speed, and the relative importance of the orienting field $\chi_R = \Omega_c\tau_R$.

We simplify the analysis by focusing only on the steady state solutions and consider fields that are either normal or parallel to the walls. We only consider linear speed variations normal to wall; hence, for a wall normal and parallel directions $\mathbf{e}_x$ and $\mathbf{e}_y$, the speed varies only along x, $\mathbf{U} = U(x)\,\mathbf{q}$, where $U(x) = U_0\left\{1-\alpha_L\left(\frac{x}{L}-\frac{1}{2}\right)\right\}$, $\alpha_L \geq 0$, and the particle rotates to align with $\hat{\mathbf{H}} = \mathbf{e}_x$ or $\mathbf{e}_y$. In such fields, there is no physical mechanism to cause any variation along the wall, hence $n = n(x)$, $\mathbf{m} = \mathbf{m}(x)$, and $\mathbf{Q} = \mathbf{Q}(x)$. Also, in wall normal fields, there cannot be any polar order along the walls $\mathbf{m} = m_x(x)\,\mathbf{e}_x$ and the nematic order is diagonal $\mathbf{Q} = Q_{xx}(x)\,\mathbf{e}_x\mathbf{e}_x - \frac{Q_{xx}(x)}{(d-1)}(\mathbf{I} - \mathbf{e}_x\mathbf{e}_x)$. Nematic order must be non-zero along the walls as $\mathbf{Q}$ is trace-free.

In general, in this problem nematic order is small ($\ll n$) everywhere except possibly at the walls and there it remains small provided that Péclet numbers are modest $\text{Pe} < 10^3$ and the effects of the external fields are not dominant $\alpha_L < 1, \chi_R < 1$. See Fig. S2 in the ESI† where we plot the nematic order as a function of position for various values of Pe, α_L, and χ_R, obtained from the full numerical solution of the Smoluchowski equation. Focusing (unless otherwise specified) on this range of parameter values, we neglect the nematic order, assuming $\mathbf{Q} = \mathbf{0}$, to develop an analytical theory.

Active matter systems tend to have reasonably high Péclet numbers[44], in which case the dominant transport process depends on the vicinity from the walls. In the bulk, away from the walls, advection is dominant, but near the walls, both advection and diffusion are equally important. To capture this, we perform a singular perturbation in Pe^{-1} and solve (2), and (3) separately in the bulk and in the near wall boundary layer (BL) regions, with an appropriate matching of the resulting solutions. This perturbative analysis is valid provided the BL thickness λ^{-1} is small relative to the channel width L, $\lambda^{-1} \ll L$, in other words $\text{Pe}\,L/\ell \gg 1$ because $\lambda \sim \text{Pe}/\ell$.

3 Fields normal to walls

Regardless of Pe, there cannot be any particle flux normal to the walls, not just at the walls but anywhere in the domain, $\mathbf{n}\cdot\mathbf{j}_n = j_{n,x} = 0\ \forall\mathbf{x}$. To derive this, integrate (2), $\nabla\cdot\mathbf{j}_n = \frac{d}{dx}j_{n,x} = 0$ using the constraint $\mathbf{n}\cdot\mathbf{j}_n|_{\text{wall}} = j_{n,x}|_{\text{wall}} = 0$.

In the bulk, neglecting translational diffusion in the flux $\mathbf{j}_n = j_{n,x}\mathbf{e}_x = \mathbf{0}$, we get $U(x)\,m_x = 0$. Assuming the self-propulsion speed is never zero, we find that there is no polar order in the bulk, $m_x = 0$. This is unlike the situation in the absence of walls, where net polar order exists in the presence of an orienting field[14], causing a finite particle flux. As there cannot be any particle flux in the

presence of walls at steady state, there cannot be any polar order in the bulk either. Similarly, neglecting polar order and diffusion in the bulk in (3) we obtain

$$\frac{d}{dx}\left(nU\left(x\right)\right)-\Omega_c n\left(d-1\right)=0. \tag{6}$$

The solution of this equation furnishes the number density in the bulk.

Unlike in the bulk, there tends to be polar order at the walls. Particles accumulate at the walls due to their persistent motion and on average, they are aligned into the walls simply because those aligned out of the walls swim away. However, the addition of strong enough orienting field can be used to rotate the particles away from the walls, ultimately preventing any wall accumulation. This points to a possible mechanism to prevent the contamination of surfaces. For instance, one could prevent the accumulation of magnetotactic bacteria *Magnetococcus marinus* through the application of strong magnetic field normal to the surface.

To examine the boundary layer at the left wall, we rescale the position with the BL thickness, $\bar{x}=\lambda_l\ell x$. We eliminate m_x from $\mathbf{j}_n=\mathbf{0}$ and (3), and evaluate the speed at the left wall U_l to obtain

$$\left(\frac{U_l}{U_0^2 d}+\frac{(d-1)}{\mathrm{Pe}U_l}\right)\frac{1}{\ell^2}\frac{dn}{d\bar{x}}-\frac{\lambda_l^2\ell^2}{\mathrm{Pe}^2U_l}\frac{d^3n}{d\bar{x}^3}-\frac{\chi_R}{\lambda_l\ell U_0}\frac{n}{\ell^3}\left(1-\frac{1}{d}\right)=0 \tag{7}$$

Balancing advection with diffusion in this equation gives the BL thickness at the left wall $\lambda_l^2\ell^2\sim\mathrm{Pe}^2\left(\frac{U_l^2}{U_0^2 d}+\frac{(d-1)}{\mathrm{Pe}}\right)$. The BL thickness is the same at both walls in the absence of the fields, $\lambda^{-1}=\lambda_l^{-1}=\lambda_r^{-1}$. On the other hand, balancing the reorientation with the diffusion gives the strength of the orienting field that is required to prevent any accumulation at the left wall, $\chi_R\sim\frac{\lambda_l^3\ell^3U_0}{\mathrm{Pe}^2U_l}\sim\mathrm{Pe}$. Similar analysis can also be carried out in the BL at the right wall.

We solve the equations in the bulk and those in the BLs and form a composite expansion. We do this calculation in a number of limits, namely: no external fields $(U=U_0,\chi_R=0)$, a weak speed modulating field $(\chi_R=0,\alpha_L\ll1)$, and also a moderate orienting field $(U=U_0,\ \chi_R<1)$. This theory is not valid for strong orienting fields $(U=U_0,\ \chi_R\gg1)$ as nematic order becomes large and cannot be neglected; thus, we develop an alternative theory for strong orienting fields. We validate these theories by comparing them with 2D Brownian Dynamics (BD) simulations. See Secs. I, II in ESI†, respectively, for the exact theoretical expressions and the BD simulation procedure.

3.1 No external fields

In the absence of any external field, the self-propulsion speed $U=U_0$ and the reorientation parameter $\chi_R=0$. Then in the bulk, while the polar order is zero, the number density satisfies $nU=constant$ or simply $n=constant$ from (6) (see also Fig. 2). On the other hand, at the walls, the particles accumulate and align into the walls, hence, $m_x<0$ at the left wall and $m_x>0$ at the right wall. Both the number density and polar order at the walls increase while the thickness of the boundary layer decreases

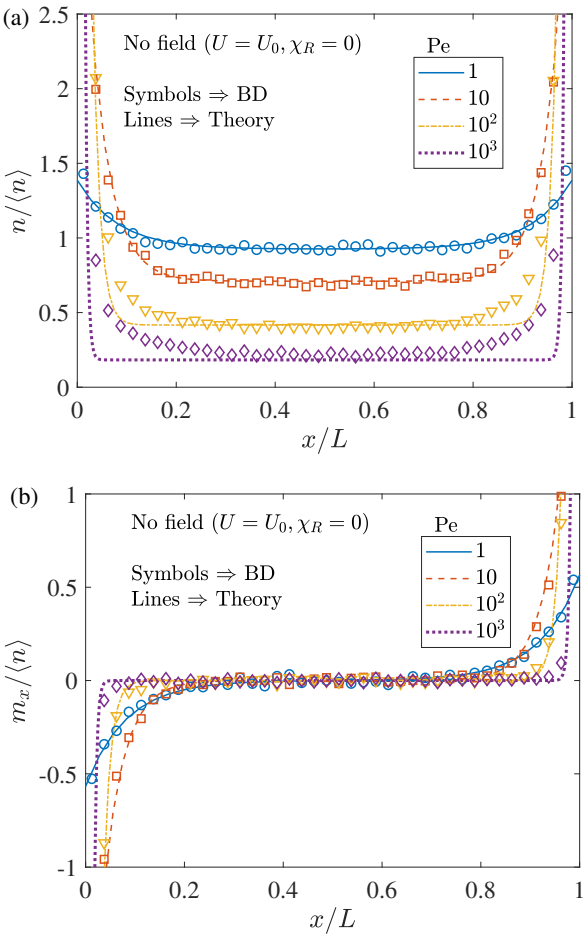

Fig. 2 In the absence of any field, the number density (a) and the polar order (b) associated with the active matter system. Here, the symbols denote the BD simulation results while the lines represent the theory (see (5), (6) in ESI†). Also, the confinement region L is 10 times larger than the microscopic length $\delta=\sqrt{D_T\tau_R}$.

with increasing Pe, $\left(\lambda^{-1}\sim\ell/\mathrm{Pe}\right)$, while the bulk concentration decreases to conserve the total number density. In this limit, the theory developed here is consistent with previous works[22,27]. It is also in agreement with Brownian dynamics simulations at moderate Pe; at very high Pe the theory breaks down due to the failure of the zero nematic order closure used.

When active particles collide with walls they exert a force or pressure ($\sim$ force/area) on them. In the absence of external fields, the pressures exerted on the left wall and the right wall are the same, $\Pi^{LW}=n^{LW}k_BT=\Pi^{RW}=n^{RW}k_BT$, where n^{LW}, n^{RW} are the number densities at the left and right walls, respectively. This wall pressure is the sum of the osmotic pressure in the bulk and the swim pressure

$$\Pi^W=\Pi^{LW}=\Pi^{RW}=n^{bulk}\left(k_BT+k_sT_s^0\right). \tag{8}$$

This formula simplifies in the high activity limit $(\mathrm{Pe}\gg1)$ after relating the bulk concentration n^{bulk} to the average concentration

$\langle n\rangle = \frac{1}{L}\int_0^L n\,dx$ as [27]

$$\Pi^W = \frac{\langle n\rangle\left(k_BT + k_sT_s^0\right)}{1+\frac{2\ell}{L\sqrt{d}(d-1)}}. \tag{9}$$

Here, the particle activity is defined as $k_sT_s^0 = \mathrm{Pe}\,k_BT/d\,(d-1) = \zeta U_0^2\tau_R/d\,(d-1)$, where ζ is the drag coefficient, k_B is the Boltzmann constant and T is the absolute temperature.

3.2 Spatially varying speed

In the presence of a field that modulates the speed spatially, say $U = U_0\left\{1-\alpha_L\left(\frac{x}{L}-\frac{1}{2}\right)\right\}$ but with $\chi_R = 0$, the bulk polar order is still zero while the number density follows $nU = constant$ scaling from (6). This means that the particles in the bulk accumulate in the regions of low speed (see Fig. 3a). Additionally, the particles also accumulate at the walls. However, unlike in the bulk where the concentration decreases with increasing speed, the number density at the walls increases with higher particle speeds. Essentially this is because faster particles travel more quickly to the walls in comparison to slower ones.

The speed and hence, the accumulation at the left wall increases (and those at the right wall decrease) with an increase in the field strength α_L. These accumulated particles exert a pressure on the walls, and hence the pressure on the left and right walls correspondingly increase and decrease with increasing field strength (see Fig. 3c). In weak fields ($\alpha_L \ll 1$), the wall pressure is again the sum of the bulk osmotic pressure and the swim pressure, but evaluated at the wall

$$\begin{aligned}\Pi^{LW} &= n^{bulk,LW}\left(k_BT + k_sT_s^{LW}\right),\\ \Pi^{RW} &= n^{bulk,RW}\left(k_BT + k_sT_s^{RW}\right),\end{aligned} \tag{10}$$

and it simplifies at high activities ($\mathrm{Pe}\gg 1$) to

$$\frac{\Pi^{LW}}{U_l/U_0} = \frac{\Pi^{RW}}{U_r/U_0} = \frac{\langle n\rangle\left(k_BT + k_sT_s^0\right)}{\frac{1}{\alpha_L}\ln\left(\frac{U_l}{U_r}\right)+\frac{2\ell}{L\sqrt{d}(d-1)}}. \tag{11}$$

Here, the activity k_sT_s is defined locally as $k_sT_s = \zeta U(x)^2\tau_R/d\,(d-1)$ and it simplifies in the absence of field to $k_sT_s^0 = \zeta U_0^2\tau_R/d\,(d-1)$. The pressure imbalance $\left(\Pi^{LW}\neq\Pi^{RW}\right)$ and the resultant net force from the walls is balanced by the net swim force (that acts as a body force [24]), which can arise due to spatial variations in speed [50], or orientation bias [24] as discussed below.

3.3 Particles in orienting fields

In an orienting field ($U = U_0, \chi_R \neq 0$), the particles rotate to align with the field for $\chi_R > 0$. Then, while the bulk polar order has to be zero to enforce the zero particle flux at steady state, the number density follows the exponential distribution from (6), $n = constant\cdot e^{(d-1)\chi_R x/\ell}$. This means the particles in bulk accumulate in the field direction or at right for $\chi_R > 0$ (See Fig. 4a). When $\chi_R = 0$ particles accumulate equally at both walls, but as χ_R increases, the accumulation at the right wall is increased while that at the left wall is diminished as particles are driven from left to right, the concentration and polar order thus become increasingly asymmetric as χ_R increases (see Fig. 4a and Fig. 4b).

The pressure exerted by the particles on the walls follows the same trend as the accumulation i.e., the pressure on the left and right walls, respectively, decrease and increase with increasing field strength χ_R (see Fig. 4c). Again, a simple expression for the wall pressure can be found in the limit of high activity ($\mathrm{Pe}\gg 1$) and weak field ($\chi_R \ll 1$)

$$\frac{\Pi^{LW}}{e^{-\kappa}} = \frac{\Pi^{RW}}{e^{\kappa}} = \frac{\langle n\rangle\left(k_BT + k_sT_s^0\right)}{\frac{\sinh\kappa}{\kappa}+\frac{2\ell}{L\sqrt{d}(d-1)}\cosh\kappa}, \tag{12}$$

where $\kappa = \chi_R\,(d-1)\,L/2\ell$.

3.4 Strong orienting fields

In strong orienting fields ($\chi_R \gg 1$), the nematic order at the right wall becomes important and hence cannot be neglected. See Fig. S2c in ESI†. As the theory developed here relies on the zero nematic order closure, it is not valid in this situation. However, some physical insights can still be drawn by applying the current theory in the strong field limit. In strong fields, for $\chi_R > 0$, we expect all the particles to align with the field, leave the left wall, and accumulate at the right wall. Hence, the left wall should be free of any particles while the accumulation at the right wall should asymptote to a value determined from the balance between the particle advection and diffusion there $\left(nU_0 \sim D_T\frac{dn}{dx}\right)$. Similarly, the pressure acting on the left wall should be zero and that acting on the right wall should asymptote to a value that depends on the particle accumulation there. We next confirm these predictions by developing an alternative theory modeling the strong field limit.

Most particles in strong orienting fields ($\chi_R \gg 1$) are aligned along the field. Hence, we approximate the probability density in this case as $P(\mathbf{x},\mathbf{q}) = n(\mathbf{x})\,\delta\left(\mathbf{q}-\hat{\mathbf{H}}\right)$, where δ is the Dirac delta function [51,52]. This reduces the polar and nematic order to $m_x = n$, $Q_{xx} = n\left(1-\frac{1}{d}\right)$. Using these, we solve (2) by enforcing the constraints $\mathbf{n}\cdot\mathbf{j}_n|_{\mathrm{wall}} = 0$ and $\frac{1}{L}\int n\,d\mathbf{x} = \langle n\rangle$, to ultimately find the number density that is correct at any $\mathrm{Pe} \leq O(\chi_R)$

$$\frac{n}{\langle n\rangle} = \frac{\mathrm{Pe}\,L/\ell}{\left(e^{\mathrm{Pe}\,L/\ell}-1\right)}e^{\mathrm{Pe}\,x/\ell}. \tag{13}$$

However, in the limit where the earlier singular perturbation analysis is valid, $\mathrm{Pe}L/\ell \gg 1$, the number density simplifies to

$$\frac{n}{\langle n\rangle} = \mathrm{Pe}\,L/\ell\,e^{-\mathrm{Pe}(L-x)/\ell}. \tag{14}$$

This equation predicts the particles are confined in a BL of thickness ℓ/Pe at the right wall (see Fig. 4a). There are no particles left in the bulk or at the left wall, hence the pressure acting on the left wall is zero. On the other hand, the pressure exerted on the right wall can be found from (14) as

$$\Pi^{LW} = 0,\ \Pi^{RW} = \mathrm{Pe}\,\frac{L}{\ell}\,\langle n\rangle\,k_BT = d\,(d-1)\,\frac{L}{\ell}\,\langle n\rangle\,k_sT_s^0. \tag{15}$$

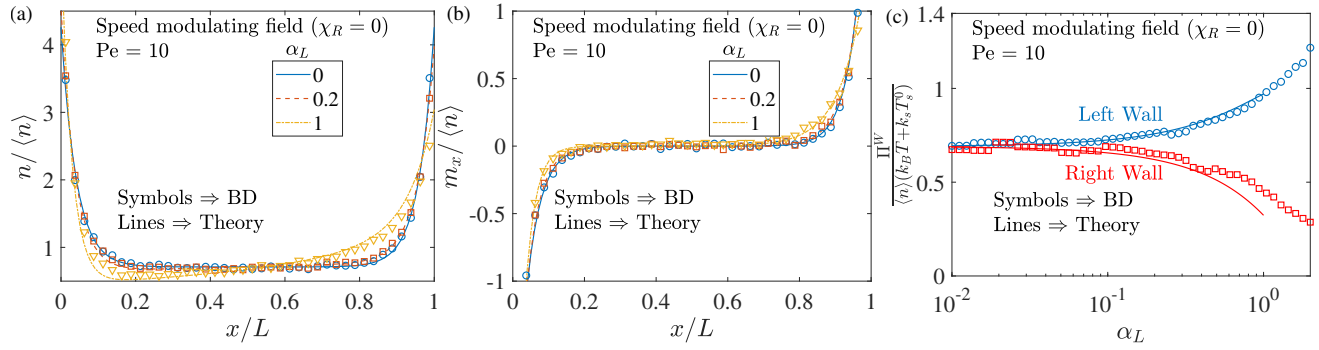

Fig. 3 The number density (a), the polar order (b), and the wall pressure (c) associated with the active matter subjected to the speed modulating field normal to the walls. The symbols denote the BD simulation results while the lines represent the theory. The confinement region L is 10 times larger than the microscopic length $\delta = \sqrt{D_T \tau_R}$.

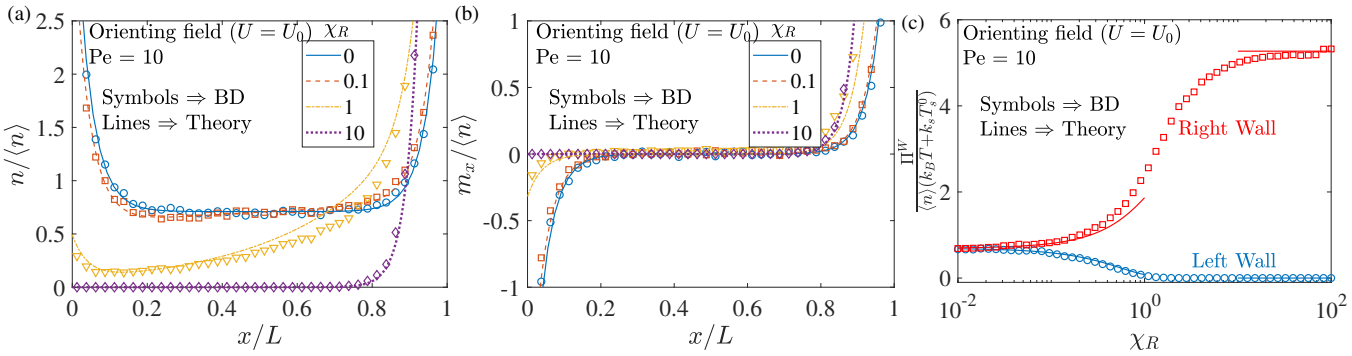

Fig. 4 The number density (a), the polar order (b), and the wall pressure (c) associated with the active matter subjected to the orienting field normal to the walls. The symbols denote the BD simulation results while the lines represent the theory. The confinement region L is 10 times larger than the microscopic length $\delta = \sqrt{D_T \tau_R}$.

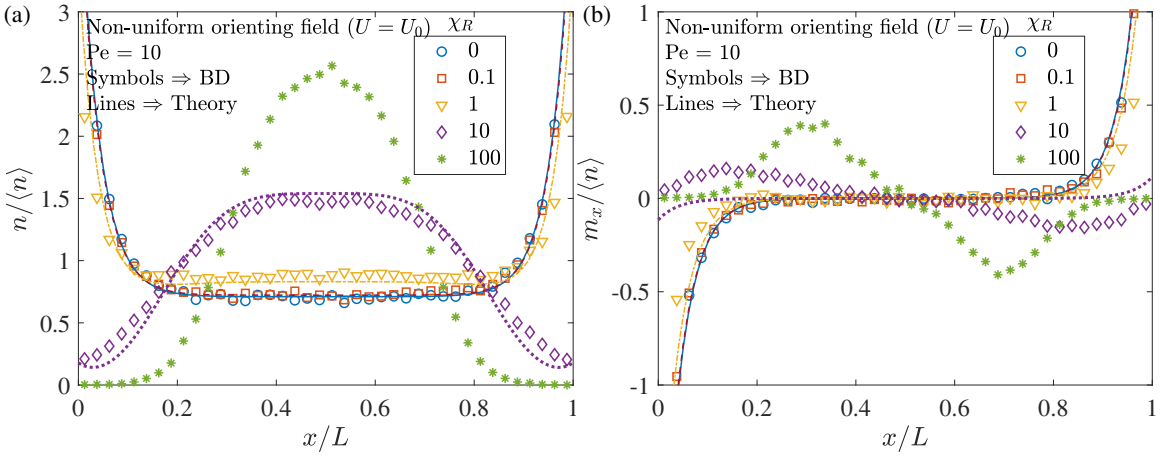

Fig. 5 The number density (a) and the polar order (b) associated with the active matter subjected to non-uniform orienting field normal to the walls, $\mathbf{H} = -(2x/L-1)^3\,\hat{\mathbf{H}}$. The symbols denote the BD simulation results while the lines represent the theory. The confinement region L is 10 times larger than the microscopic length $\delta = \sqrt{D_T \tau_R}$.

3.5 Non-uniform orienting fields

In the uniform orienting fields $\mathbf{H} = \hat{\mathbf{H}}$, we discussed how the particles rotate to align with the field, ultimately leaving one wall and accumulating at the other wall in strong fields. This suggested the potential use of orienting fields in preventing accumulation at one of the walls. We can also prevent accumulation at both walls by using a non-uniform orienting field $\mathbf{H} = H(x)\,\hat{\mathbf{H}}$, where $H(x)$ is an odd function relative to the centerline $x = L/2$ i.e., $H\left(\frac{L}{2} - x\right) = -H\left(x - \frac{L}{2}\right)$. For $H(0) > 0$, this field points away from both walls, towards the center. In such fields, the particles

rotate with velocity $\mathbf{\Omega} = \Omega_c H(x)\left(\mathbf{q}\times\hat{\mathbf{H}}\right)$ to align with the field, ultimately leaving both walls and accumulating at the center if the field is strong enough. We demonstrate this behavior for a cubic function $H(x) = -(2x/L-1)^3$ in Fig. 5, where we see that the particles indeed move from the walls towards the center as the field strength χ_R increases. A moderate field theory ($\chi_R \ll \mathrm{Pe}$) for non-uniform fields can also be developed by simply replacing the constant angular velocity Ω_c or χ_R in the formulae for uniform field ((3), (6), (7)) with $\Omega_c H(x)$ or $\chi_R H(x)$. This still yields zero polar order in the bulk but a different number density $n = constant \cdot e^{\chi_R(d-1)\int H(x)dx/\ell}$.

3.6 Combined effects

With both speed modulating and uniform orienting fields, the physics is a combination (not necessarily a linear combination) of that for the individual fields. To illustrate this, we consider the behavior in the bulk. Here, with the speed modulating field, we know the particles accumulate in the regions of low speed. Hence, for a speed decreasing from left to right, the particles accumulate at right. On the other hand, in the orienting field, for $\chi_R < 0$, the particles rotate to align against the field and accumulate in the upstream of the field (left). Then in both fields, the particles either accumulate in the regions of low speed (right) or in the upstream of the orienting field (left) depending on the relative magnitude of the field strengths (χ_R/α_L). Also, there can be no accumulation at all ($n = constant$) if the opposing effects of the fields cancel each other. This discussion is indeed consistent with the exact expression for number density found from (6)

$$n = \frac{constant}{U^{1+(d-1)\chi_R L/\ell\alpha_L}}, \tag{16}$$

where χ_R/α_L has to be $-\ell/(d-1)L$ in order for the fields to cancel each other. Also, as expected, this number density simplifies to $n = constant$ in the absence of both fields $(\chi_R, \alpha_L) \to (0,0)$ and to $nU = constant$ or $n = constant \cdot e^{(d-1)\chi_R x/\ell}$ in the presence of the speed modulating field $\chi_R \to 0$ or the orienting field $\alpha_L \to 0$, respectively.

This discussion is relevant to recent experiments with *Chlamydomonas reinhardtii* in viscosity gradients[43,53]. Spatial variations of viscosity lead to both a modulation of speed and reorientation: microorganisms tend to slow down in regions of high viscosity (viscous slowdown) but also rotate to swim down the gradients (viscophobic turning). Competition between these effects then dictates particle accumulation. For instance, in weak gradients, viscophobic turning is negligible, hence the particles accumulate in the regions of high viscosity due to their low speed. But in strong gradients, viscophobic turning dominates, hence the particles rotate to swim towards low viscosity regions[45,46] and accumulate there. Abstracting the mechanism causing the speed changes and reorientation, these dynamics are nicely captured by our simple model.

4 Fields parallel to walls

In order to give a more complete picture, in this section we discuss the effects of an orienting field aligned parallel to the walls. In this case particles rotate to align with the field and walls and then while the particle flux normal to walls is still zero $j_{n,x} = 0$, that along the walls is finite $j_{n,y} \neq 0$ due to net polar order in this direction. This finite particle flux can drive the underlying fluid inducing directed flows in a microfluidic device, for example[30].

The spatial distribution of particles and their polar order depends on the orienting field strength. In moderate fields ($\chi_R < 1$), the particle concentration n and the polar order normal to wall m_x are unaffected (or weakly affected) by the field, see Figs. 6a, 6b, and also note that the equations governing these variables ((2) and (3) along $\mathbf{e}_x$) are independent of the field. Hence, as per the no-field analysis of section 3.1, the number density in the bulk is constant and the polar order m_x is zero while there is particle accumulation at the walls. The polar order along the walls m_y, however, increases with the field strength as more and more particles turn to align with the wall, see Fig. 6c. The polar order in moderate fields can be found by solving (3) along $\mathbf{e}_y$ with the known no-field number density. The solution reveals that the polar order spatial distribution is similar to that of number density – constant in the bulk where it satisfies $m_y = \chi_R n/d$ while taking larger values at the walls due to large number of particles there. When the field exceeds moderate values ($\chi_R > 1$), wall accumulation decreases and the bulk concentration increases, because polar order normal to the walls decreases as polar order parallel to the walls increases and hence particles are more likely to leave the walls by rotary diffusion. In strong fields ($\chi_R \gg 1$), all particles are aligned with the walls and there is no wall accumulation, $n = \langle n\rangle$, $m_x = 0$, $m_y = \langle n\rangle$.

In order to capture the dependence of number density n and polar order m_x on the orienting field analytically, we must consider nematic order, which by way of (1) satisfies

$$\frac{\partial \mathbf{Q}}{\partial t} + \nabla\cdot\mathbf{j}_Q + 2dD_R\mathbf{Q} - \Omega_c\left(\hat{\mathbf{H}}\mathbf{m} + \mathbf{m}\hat{\mathbf{H}}\right) + 2\Omega_c\hat{\mathbf{H}}\cdot\mathbf{B} + \frac{2}{d+2}\Omega_c\hat{\mathbf{H}}\cdot\boldsymbol{\alpha}\cdot\mathbf{m} = \mathbf{0}, \tag{17}$$

where

$$\mathbf{j}_Q = \int \mathbf{j}_T\,\overline{\mathbf{qq}}\,d\mathbf{q} = U(\mathbf{x})\,\mathbf{B} + \frac{U(\mathbf{x})}{d+2}\boldsymbol{\alpha}\cdot\mathbf{m} - \frac{U(\mathbf{x})}{d}\mathbf{m}\mathbf{I} - D_T\nabla\mathbf{Q}, \tag{18}$$

$\mathbf{B} = \int P\overline{\mathbf{qqq}}\,d\mathbf{q}$, and $\alpha_{ijkl} = \delta_{ij}\delta_{kl} + \delta_{ik}\delta_{jl} + \delta_{il}\delta_{jk}$. We then close equations by neglecting the next higher order moment, $\mathbf{B} = \mathbf{0}$. As usual, we neglect diffusion and set m_x to zero in the bulk. We eliminate nematic order from (2), (3), and (17) to derive a relationship between the number density and the polar order

$$n - \frac{3\chi_R}{2(d+2)}m_y = constant. \tag{19}$$

As the relative field increases thereby increasing polar order m_y in the bulk, (19) tells us that the concentration in the bulk must also increase, and in order to conserve particle number wall accumulation must then proportionally decrease as shown in Figs. 6a, 6b, 6c.

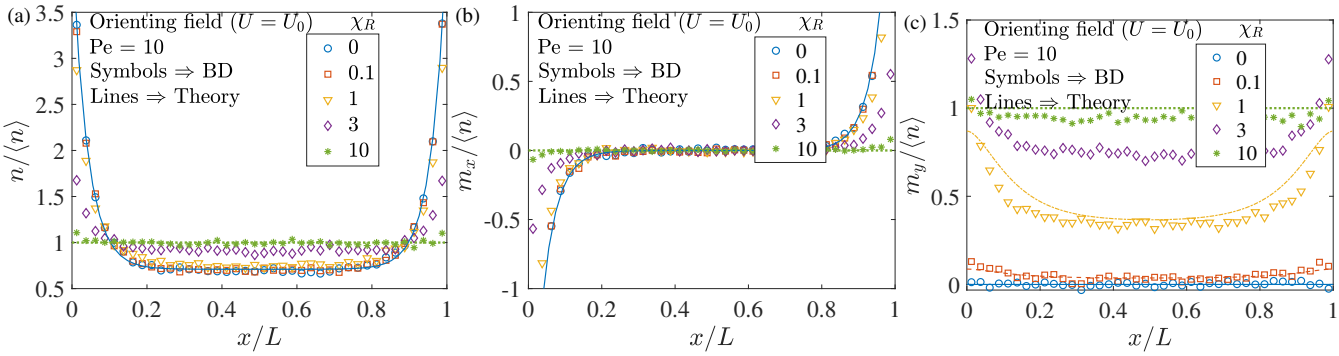

Fig. 6 The number density (a), and the polar order (b), (c) associated with the active matter subjected to an orienting field parallel to the walls. The symbols denote the BD simulation results while the lines represent the theory. The confinement region L is 10 times larger than the microscopic length $\delta = \sqrt{D_T \tau_R}$.

5 Conclusions

In summary, we analyzed confined active matter subjected to speed modulating and orienting fields. We showed that bulk polar order in the wall normal direction is always zero while the number density satisfied the usual $nU = constant$ scaling in the speed modulating fields but a different exponential distribution in orienting fields. The particles usually accumulate at the walls, but the orienting fields can be used to turn the particles away from the wall, ultimately preventing the accumulation at a wall. We also discussed the force exerted by the active matter on the confining walls and provided a concise expressions for the wall pressure.

Here we have neglected hydrodynamic interactions between the active particles and a natural next step is to include them. Hydrodynamic interaction between active particles are generally dipolar to leading order (in a dilute system) and hence mediated by the $\mathbf{Q}$ tensor field[47], which therefore cannot be neglected and more sophisticated closures (besides simple truncation) are generally used to ameliorate the hierarchy problem associated with projection of the Smoluchoswki equation onto moments[52,54]. Hydrodynamic interactions will also modify the resistance as well as the diffusivity (for Brownian particles)[26], but many-body hydrodynamic interactions can be computed numerically[55].

Conflicts of interest

There are no conflicts to declare.

Acknowledgements

G.J.E. acknowledges the hospitality of the Division of Chemistry and Chemical Engineering at the California Institute of Technology during a sabbatical stay that served as a formative period of this work. This work was supported the National Science Foundation (J.F.B., grant no. CBET 1803662), the Natural Sciences and Engineering Research Council of Canada (G.J.E., grant no. RGPIN-2020-04850) and by a UBC Killam Research Fellowship to G.J.E.

References

1 S. Ramaswamy, *Annu. Rev. Condens. Matter Phys.*, 2010, **1**, 323–345.
2 M. C. Marchetti, J. F. Joanny, S. Ramaswamy, T. B. Liverpool, J. Prost, M. Rao and R. A. Simha, *Rev. Mod. Phys.*, 2013, **85**, 1143–1189.
3 C. Bechinger, R. Di Leonardo, H. Löwen, C. Reichhardt, G. Volpe and G. Volpe, *Rev. Mod. Phys.*, 2016, **88**, 045006.
4 S. Ramaswamy, *J. Stat. Mech.: Theory Exp.*, 2017, **2017**, 054002.
5 D. Needleman and Z. Dogic, *Nat. Rev. Mater.*, 2017, **2**, 17048.
6 J. Toner, Y. Tu and S. Ramaswamy, *Ann. Phys.*, 2005, **318**, 170–244.
7 R. Alert, J. Casademunt and J.-F. Joanny, *Annu. Rev. Condens. Matter Phys.*, 2022, **13**, 143–170.
8 M. E. Cates and J. Tailleur, *Annu. Rev. Condens. Matter Phys.*, 2015, **6**, 219–244.
9 G. Volpe, I. Buttinoni, D. Vogt, H.-J. Kümmerer and C. Bechinger, *Soft Matter*, 2011, **7**, 8810.
10 I. Buttinoni, G. Volpe, F. Kümmel, G. Volpe and C. Bechinger, *J. Phys. Condens. Matter*, 2012, **24**, 284129.
11 J. Palacci, S. Sacanna, A. P. Steinberg, D. J. Pine and P. M. Chaikin, *Science*, 2013, **339**, 936–940.
12 T. D. Ross, H. J. Lee, Z. Qu, R. A. Banks, R. Phillips and M. Thomson, *Nature*, 2019, **572**, 224–229.
13 R. Zhang, S. A. Redford, P. V. Ruijgrok, N. Kumar, A. Mozaffari, S. Zemsky, A. R. Dinner, V. Vitelli, Z. Bryant, M. L. Gardel and J. J. de Pablo, *Nat. Mater.*, 2021, **20**, 875–882.
14 S. C. Takatori and J. F. Brady, *Soft Matter*, 2014, **10**, 9433–9445.
15 M. A. Fernandez-Rodriguez, F. Grillo, L. Alvarez, M. Rathlef, I. Buttinoni, G. Volpe and L. Isa, *Nat. Commun.*, 2020, **11**, 4223.
16 J. O. Kessler, *Nature*, 1985, **313**, 218–220.
17 J. Arlt, V. A. Martinez, A. Dawson, T. Pilizota and W. C. K. Poon, *Nat. Commun.*, 2018, **9**, 768.
18 M. J. Schnitzer, *Phys. Rev. E*, 1993, **48**, 2553–2568.
19 J. Tailleur and M. E. Cates, *Phys. Rev. Lett.*, 2008, **100**, 218103.
20 M. E. Cates and J. Tailleur, *Europhys. Lett.*, 2013, **101**, 20010.

21 J. Arlt, V. A. Martinez, A. Dawson, T. Pilizota and W. C. K. Poon, *Nat. Commun.*, 2019, **10**, 2321.

22 H. Row and J. F. Brady, *Phys. Rev. E*, 2020, **101**, 062604.

23 B. Ezhilan and D. Saintillan, *J. Fluid Mech.*, 2015, **777**, 482–522.

24 W. Yan and J. F. Brady, *Soft Matter*, 2015, **11**, 6235–6244.

25 A. P. Solon, Y. Fily, A. Baskaran, M. E. Cates, Y. Kafri, M. Kardar and J. Tailleur, *Nat. Phys.*, 2015, **11**, 673–678.

26 E. W. Burkholder and J. F. Brady, *Soft Matter*, 2018, **14**, 3581–3589.

27 W. Yan and J. F. Brady, *J. Fluid Mech.*, 2015, **785**, R1.

28 S. C. Takatori, W. Yan and J. F. Brady, *Phys. Rev. Lett.*, 2014, **113**, 028103.

29 W. Yan and J. F. Brady, *New J. Phys.*, 2018, **20**, 053056.

30 R. Alonso-Matilla and D. Saintillan, *Europhys. Lett.*, 2018, **121**, 24002.

31 J. Hill, O. Kalkanci, J. L. McMurry and H. Koser, *Phys. Rev. Lett.*, 2007, **98**, 068101.

32 T. Kaya and H. Koser, *Phys. Rev. Lett.*, 2009, **103**, 138103.

33 T. Kaya and H. Koser, *Biophys. J.*, 2012, **102**, 1514–1523.

34 V. Kantsler, J. Dunkel, M. Blayney and R. E. Goldstein, *eLife*, 2014, **3**, e02403.

35 Z. Peng and J. F. Brady, *Phys. Rev. Fluids*, 2020, **5**, 073102.

36 R. Rusconi, J. S. Guasto and R. Stocker, *Nat. Phys.*, 2014, **10**, 212–217.

37 S. Chilukuri, C. H. Collins and P. T. Underhill, *Phys. Fluids*, 2015, **27**, 031902.

38 I. Frankel and H. Brenner, *J. Fluid Mech.*, 1989, **204**, 97–119.

39 L. Fung, R. N. Bearon and Y. Hwang, *J. Fluid Mech.*, 2022, **935**, A24.

40 R. N. Bearon, A. L. Hazel and G. J. Thorn, *J. Fluid Mech.*, 2011, **680**, 602–635.

41 R. N. Bearon and A. L. Hazel, *J. Fluid Mech.*, 2015, **771**, R3.

42 A. Zöttl and H. Stark, *Phys. Rev. Lett.*, 2012, **108**, 218104.

43 M. R. Stehnach, N. Waisbord, D. M. Walkama and J. S. Guasto, *Nat. Phys.*, 2021, **17**, 926–930.

44 S. C. Takatori, R. De Dier, J. Vermant and J. F. Brady, *Nat. Commun.*, 2016, **7**, 10694.

45 C. Datt and G. J. Elfring, *Phys. Rev. Lett.*, 2019, **123**, 158006.

46 V. A. Shaik and G. J. Elfring, *Phys. Rev. Fluids*, 2021, **6**, 103103.

47 D. Saintillan and M. J. Shelley, *C. R. Phys.*, 2013, **14**, 497–517.

48 S. Hess, *Tensors for Physics*, Springer International Publishing, Cham, 2015.

49 S. Maretvadakethope, A. L. Hazel, B. Vasiev and R. N. Bearon, *Arxiv*, 2022, 2209.05973 [physics.flu–dyn].

50 S. C. Takatori and J. F. Brady, *Phys. Rev. E*, 2015, **91**, 032117.

51 D. Saintillan and M. J. Shelley, *Phys. Fluids*, 2008, **20**, 123304.

52 T. Gao, M. D. Betterton, A.-S. Jhang and M. J. Shelley, *Phys. Rev. Fluids*, 2017, **2**, 093302.

53 S. Coppola and V. Kantsler, *Sci. Rep.*, 2021, **11**, 399.

54 S. Weady, D. B. Stein and M. J. Shelley, *Phys. Rev. Fluids*, 2022, **7**, 063301.

55 G. J. Elfring and J. F. Brady, *J. Fluid Mech.*, 2022, **952**, A19.